Cell Reports

Article

# Alpha synuclein determines ferroptosis sensitivity in dopaminergic neurons via modulation of ether-phospholipid membrane composition

## Graphical abstract

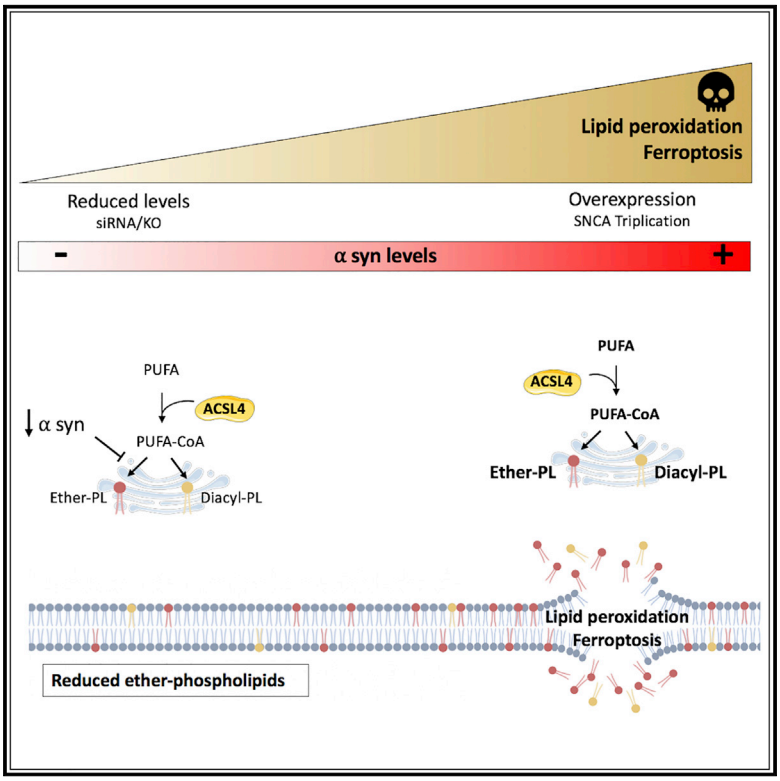


## Highlights

- α-Synuclein levels determine sensitivity of dopaminergic neurons to ferroptosis
- α-Synuclein regulates the synthesis of ether-linked phospholipids
- Elevated α-synuclein expression increases lipid peroxidation and ferroptosis risk


## Authors

Laura Mahoney-Sanchez, Hind Bouchaoui, Ibrahim Boussaad, ..., James A. Duce, David Devos, Jean-Christophe Devedjian

## Correspondence

james.duce@florey.edu.au (J.A.D.), david.devos@chru-lille.fr (D.D.)



## In brief

The pathological mechanisms underlying α-synuclein toxicity and neuronal cell death in Parkinson's disease are unclear. Mahoney-Sanchez et al. present a direct association between endogenous α-synuclein levels and the sensitivity of dopaminergic neurons to lipid peroxidation and ferroptosis via modulation of plasma membrane ether-linked phospholipids.


Mahoney-Sanchez et al., 2022, Cell Reports *40*, 111231
August 30, 2022 
https://doi.org/10.1016/j.celrep.2022.111231

CellPress

Cell Reports

CellPress
OPEN ACCESS

Article

# Alpha synuclein determines ferroptosis sensitivity in dopaminergic neurons via modulation of ether-phospholipid membrane composition

Laura Mahoney-Sanchez,[1] Hind Bouchaoui,[1] Ibrahim Boussaad,[2] Aurélie Jonneaux,[1] Kelly Timmerman,[1] Olivier Berdeaux,[3] Scott Ayton,[4] Rejko Krüger,[2,5,6] James A. Duce,[4,7,9,*] David Devos,[1,9,10,*] and Jean-Christophe Devedjian[1,8,9]

[1]Department of Medical Pharmacology, Lille University, INSERM UMRS_1772, Lille University Hospital, LICEND COEN Centre, LilNCog – Lille Neuroscience & Cognition, 59000 Lille, France
[2]Translational Neuroscience, Luxembourg Centre for Systems Biomedicine (LCSB), University of Luxembourg, 4365 Esch-sur-Alzette, Luxembourg
[3]Lipid-Aroma Platform, Centre des Sciences Du Goût et de l'Alimentation, UMR6265 CNRS, UMR1324 INRA, Université de Bourgogne, Agrosup Dijon, 21000 Dijon, France
[4]Melbourne Dementia Research Centre, Florey Institute of Neuroscience and Mental Health, The University of Melbourne, Melbourne, VIC, Australia
[5]Transversal Translational Medicine, Luxembourg Institute of Health (LIH), 1445 Strassen, Luxembourg
[6]Parkinson Reserch Clinic, Centre Hospitalier de Luxembourg (CHL), 1210 Luxembourg (Belair), Luxembourg
[7]The ALBORADA Drug Discovery Institute, University of Cambridge, Cambridge Biomedical Campus, Cambridge, UK
[8]Université Du Litoral Côte D'Opale, 1, Place de l'Yser, Dunkerque Cedex, France
[9]These authors have equally contributed
[10]Lead contact
*Correspondence: james.duce@florey.edu.au (J.A.D.), david.devos@chru-lille.fr (D.D.)
https://doi.org/10.1016/j.celrep.2022.111231

## SUMMARY

There is a continued unmet need for treatments that can slow Parkinson's disease progression due to the lack of understanding behind the molecular mechanisms underlying neurodegeneration. Since its discovery, ferroptosis has been implicated in several diseases and represents a therapeutic target in Parkinson's disease. Here, we use two highly relevant human dopaminergic neuronal models to show that endogenous levels of α-synuclein can determine the sensitivity of dopaminergic neurons to ferroptosis. We show that reducing α-synuclein expression in dopaminergic neurons leads to ferroptosis evasion, while elevated α-synuclein expression in patients' small-molecule-derived neuronal precursor cells with *SNCA* triplication causes an increased vulnerability to lipid peroxidation and ferroptosis. Lipid profiling reveals that ferroptosis resistance is due to a reduction in ether-linked phospholipids, required for ferroptosis, in neurons depleted of α-synuclein (α-syn). These results provide a molecular mechanism linking α-syn levels to the sensitivity of dopaminergic neurons to ferroptosis, suggesting potential therapeutic relevance.

## INTRODUCTION

Parkinson's disease (PD) is pathologically defined by dopaminergic neurodegeneration, α-synuclein (α-syn) aggregation, and deposition within Lewy bodies as well as iron accumulation in the substantia nigra pars compacta (SNc) (Dexter et al., 1989a; Spillantini et al., 1997; Schneider and Obeso, 2015). These pathological hallmarks have encouraged the progress of therapeutic avenues toward dopamine restoration, mitigating the aggregation of α-syn and iron chelation. Despite symptomatic relief, a huge unmet need remains for efficient disease-modifying therapies that can reduce dopaminergic neuron death and thus disease progression. To overcome this demand, a better understanding of the mechanisms involved in the development of these pathological hallmarks and their dynamic relationship to cell death is required. For many years, neuronal death in PD was considered to be caused via apoptosis (Ziv et al., 2001). This was mainly due to the fact that until recently, the use of oncogenic cell lines (e.g., neuroblastoma) greatly limited the types of regulated cell death that were able to be identified (Galluzzi et al., 2018). Since the field continues to expand, novel mechanisms that orchestrate multiple cell-death pathways have been unveiled. This is in part due to a greater use of primary cultures and the capacity to separate key differences in cell-death mechanisms, which has resulted in more cell-death processes implicated with disease mechanisms (Guiney et al., 2017; Galluzzi et al., 2018). More recently, ferroptosis was identified as a novel cell-death pathway characterized by iron-dependent lipid peroxide accumulation (Dixon et al., 2012; Stockwell et al., 2017) and is increasingly implicated in various human diseases

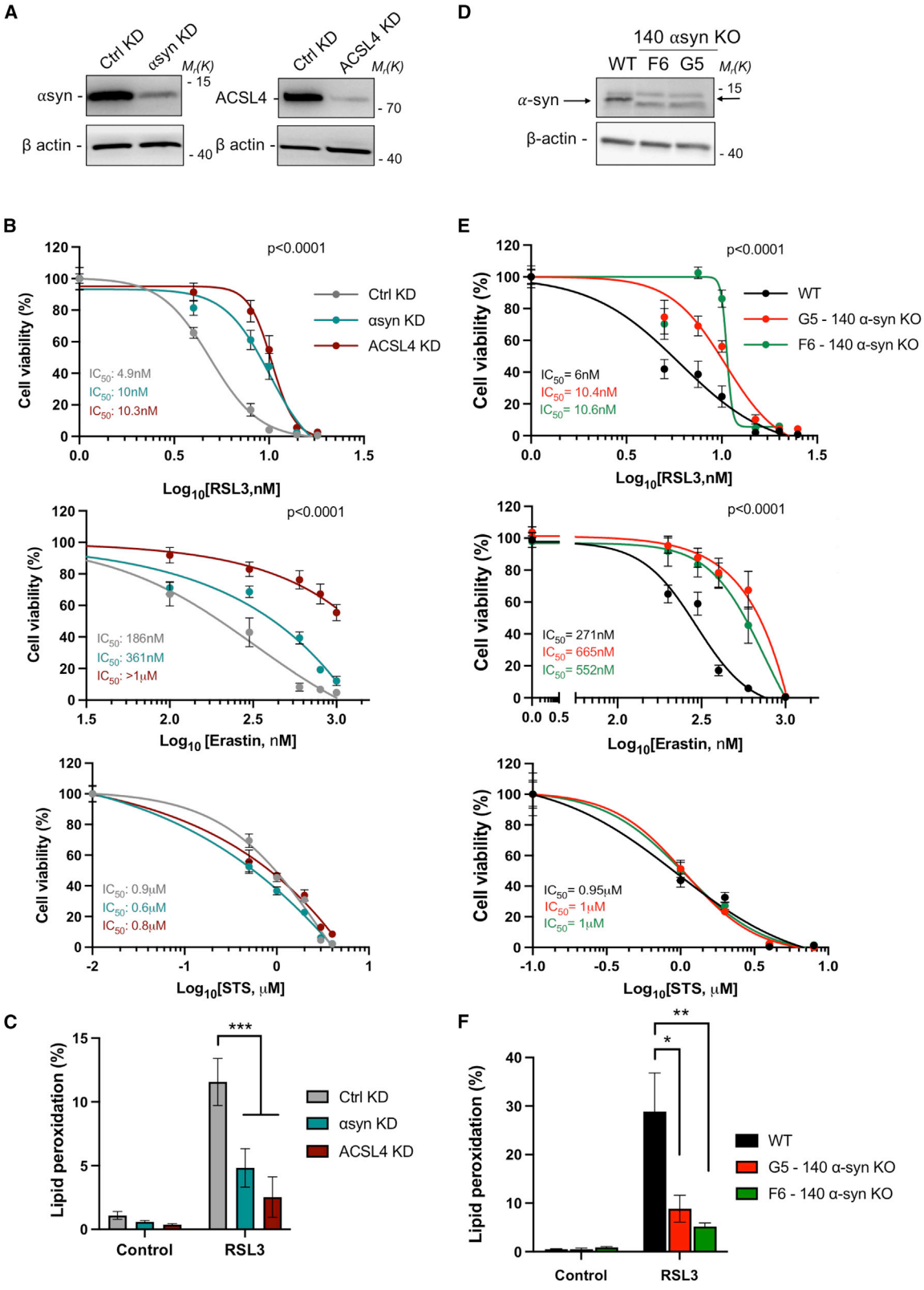


*(legend on next page)*

as well as *in vivo* disease models (Friedmann Angeli et al., 2014; Do Van et al., 2016; Martin-Sanchez et al., 2017; Karuppagounder et al., 2018; Alim et al., 2019; Devos et al., 2019). The initiation, execution, and inhibition of ferroptosis lies at the intersection of the metabolism of amino acids, lipids, and iron (Tang et al., 2021). The peroxidation of polyunsaturated fatty acids (PUFAs) in the membrane phospholipids (PLs) is a key step in promoting ferroptosis (Yang et al., 2016). Therefore, the lipid composition of the plasma membrane can determine cellular susceptibility to ferroptosis whereby long-chain PUFAs increase the risk for lipid peroxidation, while monounsaturated fatty acids (MUFAs) appear to decrease such risk (Magtanong et al., 2019). We have previously shown that ferroptosis is indeed a prevalent mechanism for neuronal cell death in *in vitro* and *in vivo* pro-oxidant models of PD (Do Van et al., 2016; Mahoney-Sánchez et al., 2020), and there is an indication that some familial patients with PD carry mutations in proteins important in modulating pathways that alter ferroptosis sensitivity (Cao et al., 2020; Vallerga et al., 2020).

In addition to being a major component of Lewy body pathology, α-syn is implicated in PD causality by genome-wide association studies of sporadic PD and autosomal dominantly inherited mutations and duplication/triplication in the *SNCA* gene that lead to various clinical phenotypes ranging from typical late-onset to rapid progressive early-onset familial PD (Zhang et al., 2018a; Blauwendraat et al., 2019). Despite the genetic support for the involvement of α-syn in PD pathology, neither the physiological function nor the neuropathological mechanisms of this protein are fully understood. In this study, we sought to investigate the potential implication of endogenous α-syn in ferroptosis sensitivity given the evidence implicating α-syn with an altered lipid metabolism, particularly the plasma membrane PUFA composition (Sharon et al., 2001, 2003; Golovko et al., 2005, 2006, 2007; Barceló-Coblijn et al., 2007). Here, we demonstrate that α-syn plays a pivotal role in dopaminergic neuron survival by regulating PL membrane composition; specifically, the ether-linked PLs (ether-PLs) essential for ferroptotic cell death (Zou et al., 2020; Cui et al., 2021). Suppression of α-syn expression markedly decreases the proportion of ether-PLs in the plasma membrane of dopaminergic neurons, increasing the resistance to ferroptosis in neurons to a comparable level as when the major ferroptotic regulator acyl-coenzyme A (CoA) synthetase long-chain family member 4 (ACSL4) is reduced. Conversely, elevated levels of α-syn in human small-molecule-derived neuronal precursor cell (smNPC)-derived midbrain neurons with *SNCA* triplication render neurons more vulnerable to ferroptosis-induced lipid peroxidation and cell death. The discovery of α-syn as a positive modulator of ferroptosis in two distinct dopaminergic neuronal models supports ferroptosis as a key mechanism involved in the pathology of PD and provides potential ferroptosis-based therapeutic opportunities in the disease.

## RESULTS

### Depletion of α-synuclein selectively protects neurons against ferroptosis

To investigate the impact of α-syn on ferroptosis, α-syn was knocked down (KD) by small interfering RNA (siRNA) in LUHMES cells (Figure 1A, S1A, and S1B), a relevant human neuronal precursor cell line that can be differentiated into a mature, post-mitotic homogeneous dopaminergic cell population. As ACSL4 is a well-established pro-ferroptotic modulator involved in enriching cellular membrane with PUFAs (Doll et al., 2017), all readouts were compared with KD of this enzyme in the same dopaminergic cell line. Reducing both α-syn and ACSL4 expression significantly protected neurons against both RSL3 and erastin-induced ferroptosis, while no difference in sensitivity was observed against staurosporin (STS)-triggered apoptosis (Figure 1B), suggesting a ferroptosis-specific effect. Of note, since α-syn modulation was still observed when ferroptosis was triggered through a downstream component (e.g., glutathione peroxidase 4 [GPX4] inhibition via RSL3), it is likely that the ferroptosis-associated mechanism involving α-syn is not upstream of GPX4. Ferroptotic cell death ultimately occurs due to a cellular imbalance in elevated lipid peroxides that outweigh the capacity for GPX4 to act as a reductant in the presence of glutathione, and thus lipid peroxidation is a classic ferroptosis biomarker. Using the specific ferroptosis-inducer RSL3 and the fluorescent probe C-11 BODIPY to measure lipid reactive oxygen species (ROS) by flow cytometry, a depletion of α-syn levels was shown to mitigate ferroptosis-dependent lipid peroxidation to a similar level as ACSL4 KD (Figure 1B).

To support the initial findings observed with acute KD of α-syn by siRNA, we established two stable cell lines that lack the main 140 amino acid isoform of α-syn (referred to as F6 and G5 −140 α-syn knockout [KO]) (Figures 1D and S2). These two isoform-specific KO cell lines were generated by CRISPR-Cas9 genome modification, whereby exon 3 in the *SNCA* locus was targeted in LUHMES cells. Through non-homologous end-joining (NHEJ) repair, the insertion of an extra guanidine that caused a shift in the reading frame (clone F6) or a deletion of 7 nucleotides (clone G5) led to alternative splicing of the *SNCA* gene (Figure S2A)

**Figure 1. Depletion of α-synuclein selectively protects dopaminergic neurons from ferroptosis comparative to ACSL4**

(A) Representative western blot analysis of α-synuclein (α-syn) and ACSL4 KD in LUHMES cells compared with control siRNA KD.

(B) Non-linear regression dose curves for viability in control (Ctrl), α-syn, and ACSL4 KD LUHMES cell upon treatment (24 h) with the ferroptosis inducers RSL3 and erastin or the apoptosis inducer staurosporine (STS). Curves were fitted, and extra sum-of-squares F tests were performed to assess whether differences were statistically significant.

(C) Lipid peroxidation as assayed by flow cytometry using the C11-BODIPY probe, in Ctrl, α-syn, or ACSL4 KD LUHMES cells treated with RSL3 (20 nM; 6 h).

(D) Representative western blot analysis of LUHMES with wild-type α-syn (WT) or two 140 α-syn KO clones.

(E) Viability curves for WT and 140 α-syn KO clones in response to treatment (24 h) with RSL3, erastin, or STS. Curves were fitted, and extra sum-of-squares F tests were performed to assess whether differences were statistically significant.

(F) Lipid peroxidation analysis of WT and 140 α-syn KO clones after treatment with RSL3 (15 nM; 24 h).

All data are represented as mean ± SEM of three independent experiments. Comparisons in (C) and (F) were made using the two-tailed, unpaired Student's t test; *p < 0.05, ** p > 0.01, ***p < 0.001.

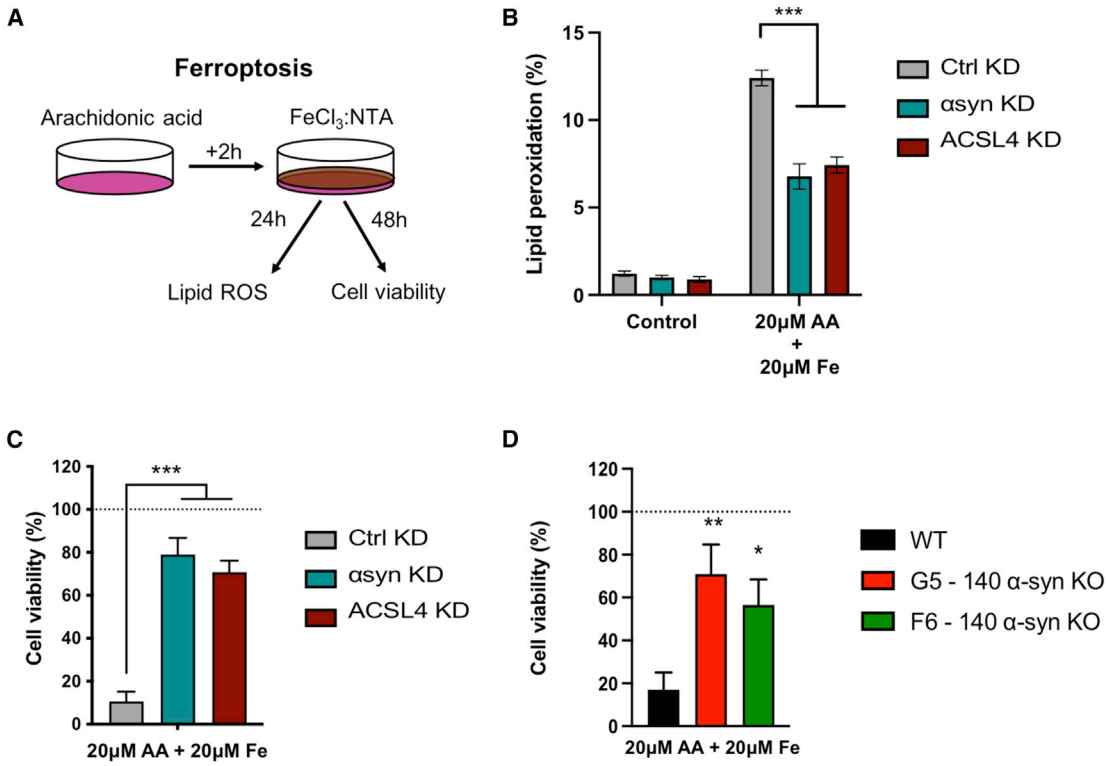


**Figure 2. α-syn and ACSL4 mediate dopaminergic neuron sensitivity to ferroptosis induced by arachidonic acid and iron**

(A) Schematic representation of a more physiologically relevant model of ferroptosis in which differentiated LUHMES cells were treated with arachidonic acid (AA) (20 μM) followed by $FeCl_3$:NTA (20 μM) before measuring lipid peroxidation or cell viability at 24 and 48 h, respectively. NTA, nitrilotriacetic acid.

(B and C) Lipid peroxidation (B) and cell viability (C) in Ctrl, α-syn, or ACSL4 KD LUHMES cells using the AA + Fe model of ferroptosis.

(D) Cell viability for WT and 140 α-syn KO LUHMES clones in response to AA + Fe co-treatment (48 h).

Results are expressed as mean ± SEM of three independent experiments. Statistical comparisons were made using two-tailed, unpaired Student's t test; *$p < 0.05$, **$p < 0.01$, ***$p < 0.001$.

that deleted the full-length 140 α-syn isoform (Figures S2B–S2D). In line with our previous findings, both 140 α-syn KO clones were found to be more resistant to ferroptosis induced by erastin and RSL3 but had no effect on apoptosis sensitivity (Figure 1E). Consistent with the KD experiments, both 140 α-syn KO subclones also exhibited reduced RSL3-induced lipid peroxidation accumulation compared with the wild-type (WT) parental line (Figure 1F).

## Arachidonic-acid- and iron-induced ferroptosis is mediated by α-synuclein expression

Two key pathological hallmarks of PD include iron overload (Dexter et al., 1989a; Ayton et al., 2015; Moreau et al., 2018) and elevated lipid peroxidation (Dexter et al., 1986, 1989b; de Farias et al., 2016) in the SNpc. Of note, impaired metabolism of fatty acids (FAs) with higher levels of membrane PUFAs are evident in both PD and dementia with Lewy bodies (DLB) postmortem brain (Sharon et al., 2003). In an attempt to model a more physiologically relevant environment to induce ferroptosis that also has relevance to PD, the abundant brain PUFA arachidonic acid (AA) and FeCl3 were studied in combination at doses that were subtoxic when administered separately (Figure 2A). Specific induction of ferroptosis cell death and lipid peroxidation has recently been confirmed in this model, and a range of known ferroptosis inhibitors (e.g., deferiprone, ferrostatin-1, and liproxstatin), as well as genetic depletion of ACSL4 or 15/15B lipoxygenases (ALOX15/15B), protect neurons against ferroptotic cell death and lipid peroxidation (Bouchaoui et al., unpublished data).

The depletion of α-syn in LUHMES neurons co-treated with AA and iron (Fe) protected against both lipid peroxide generation (Figure 2B) and cell death (Figure 2C), similar to that observed with pharmacologically induced ferroptosis (Figure 1). Levels of protection by α-syn depletion were comparable to KD of ACSL4 (Figures 2B and 2C). A similar protection against AA- and Fe-induced cell death was also observed in both 140 α-syn KO subclones (Figure 2D). Taken together, these findings, in addition to prior studies, support α-syn having a role in the metabolisms of PUFAs (Sharon et al., 2003; Barceló-Coblijn et al., 2007; Golovko et al., 2005, 2006, 2007) and subsequently indicate that α-syn specifically mediates the sensitivity of dopaminergic neurons to ferroptosis induced by the toxic combination of AA and Fe.

## α-Synuclein levels determine ferroptosis sensitivity in patient-derived midbrain neurons

To determine that observations in the LUHMES neurons were not due to a cell-specific phenotype, a second *in vitro* human

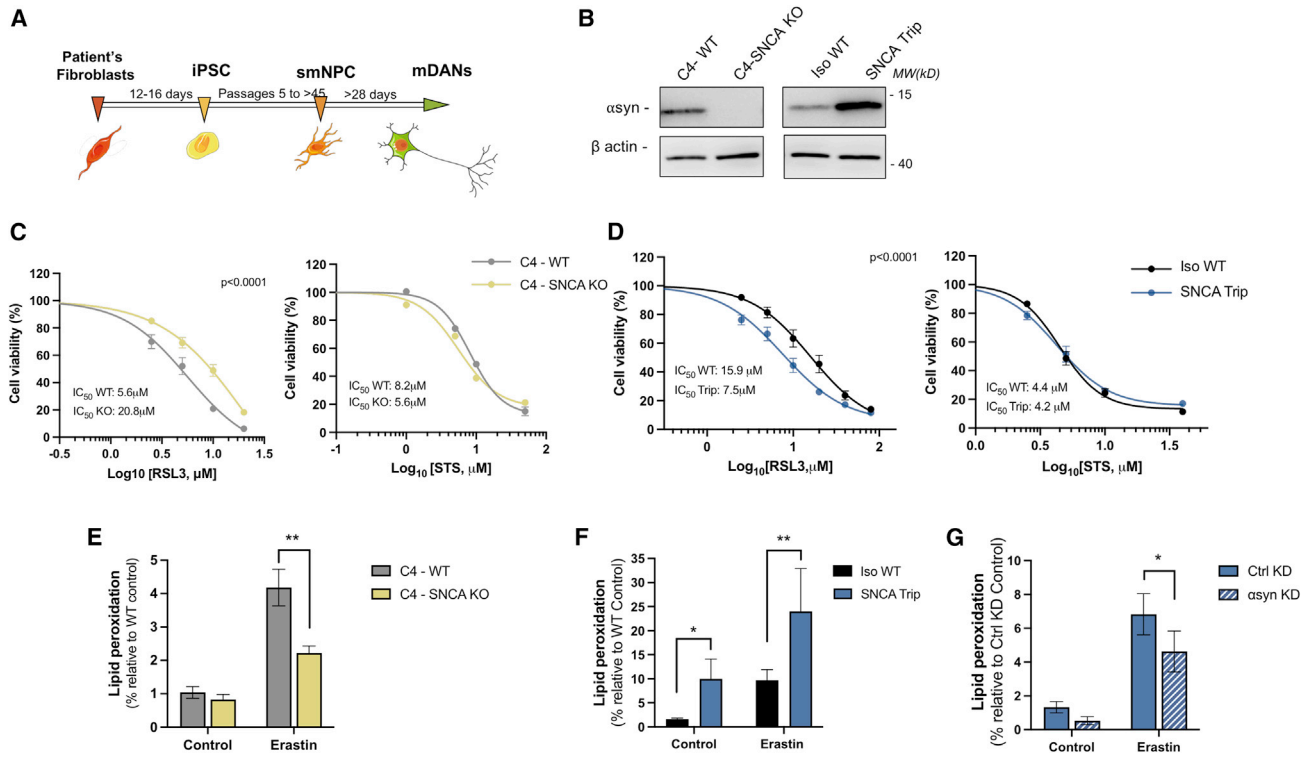


**Figure 3. α-syn enhances ferroptosis in human smNPC-derived midbrain neurons**

(A) Differentiation protocol of human fibroblast into midbrain dopaminergic neurons (mDANs).

(B) Western blot confirmation of α-syn expression in smNPC-derived midbrain neurons comparing the isogenic Ctrl (C4-WT) with a CRISPR-Cas9-generated *SNCA* KO (C4-*SNCA* KO) or familial *SNCA* triplication to its isogenic Ctrl.

(C and D) Cell viability curves for WT versus *SNCA* KO (C) and *SNCA* Trip versus isogenic WT (D) mDANs in response to RSL3 or STS (24 h). Curves were fitted, and extra sum-of-squares F tests were performed to assess whether differences were statistically significance.

(E and F) Lipid peroxidation upon erastin treatment (80 μM; 6 h) in WT and *SNCA* KO as well as isogenic WT and *SNCA* Trip human mDANs.

(G) Lipid peroxidation upon erastin treatment (80 μM; 6 h) in *SNCA* Trip mDANs transfected with α-syn siRNA relative to Ctrl KD *SNCA* Trip mDANs.

Data represent mean ± SEM in a minimum of three independent experiments. Statistical comparisons were made the one-tailed, unpaired t test (F) or two-tailed t test (E and G); *p < 0.05, **p < 0.01, ***p < 0.001.

cell model was studied. Human midbrain dopaminergic neurons (mDANs) differentiated from smNPCs (Figure 3A) were either genetically modified by CRISPR-Cas9 to knock out α-syn (C4-*SNCA* KO) or derived from a patient with a triplication in *SNCA* (*SNCA* Trip) (Figure 3B). Comparing C4-*SNCA* KO with the C4-WT isogenic control confirmed that an absence of α-syn rendered mDANs more resistant to RSL3-induced ferroptosis but had no effect on sensitivity to STS-induced apoptosis (Figure 3C). In contrast, mDANs carrying *SNCA* triplication were more vulnerable to RSL3 toxicity when compared with their isogenic control (Iso WT) despite having no observable difference in their response to STS (Figure 3D). Paralleling the selective changes to ferroptotic cell death, lipid peroxidation levels in response to ferroptosis induction was lower in the C4-*SNCA* KO mDANs (Figure 3E) and higher in the *SNCA* Trip mDANs (Figure 3F) when compared with their respective Iso WT controls. Importantly, the triplication of *SNCA* alone sufficed to trigger lipid peroxidation under basal control conditions, indicating that an increase in α-syn levels could prime the cells to be more sensitive to ferroptosis (Figure 3F). To further confirm that the observed changes to lipid peroxidation in the *SNCA* Trip neurons were specifically due to an elevation of α-syn, we performed siRNA to reduce α-syn expression back to similar levels observed in the isogenic control (Figures 3G, S3A, and S3B). As expected, knocking down α-syn in the *SNCA* Trip neurons significantly reduced the levels of ferroptosis-induced lipid peroxidation (Figure 3G). Taken together, these findings further support α-syn as a positive modulator of ferroptosis in mDANs.

## α-Synuclein modulates the composition of ether-PLs in the plasma membrane

Prior studies have shown altered FA composition in response to abnormal α-syn levels in both *in vitro* and *in vivo* models as well as human brain (Sharon et al., 2001, 2003; Golovko et al., 2005, 2006, 2007; Barceló-Coblijn et al., 2007). Overexpression of α-syn increases levels of AA, linoleic acid, and dihomo-γ-linoleic acid, while the absence of α-syn reduces the PUFA content in brain PLs (Sharon et al., 2003; Golovko et al., 2006). Based on these findings, we hypothesized that the ferroptosis-resistant phenotype observed in α-syn-depleted neurons could be due to a reduction in PUFAs present in the PLs.

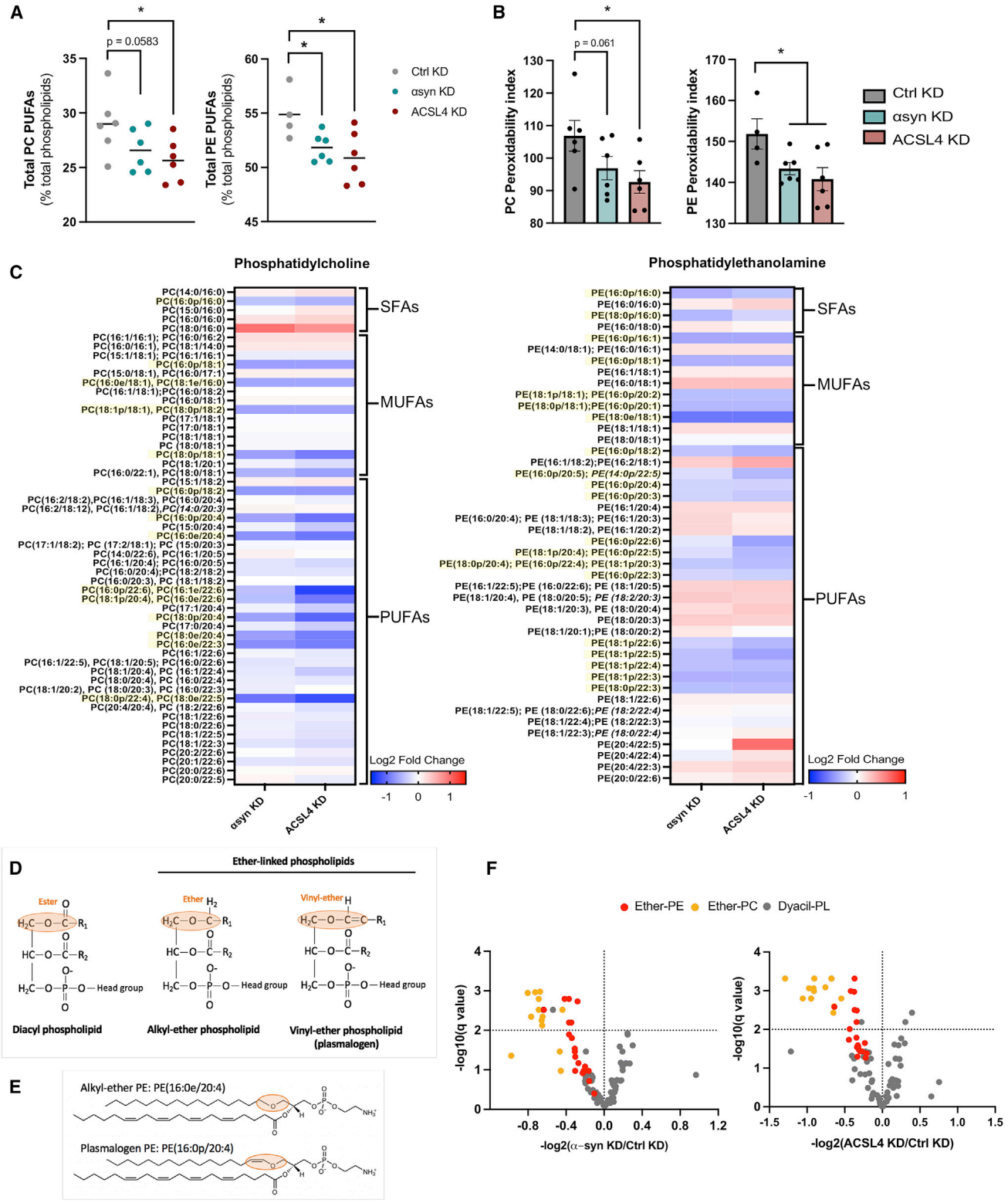


**Figure 4. Modulated ether-linked phospholipid composition by α-syn and ACSL4 expression in dopaminergic neurons**

(A and B) Total levels (A) and the peroxidability index (see STAR Methods for equation) (B) of phosphatidylcholine (PC) and phosphatidylethanolamine (PE) phospholipid containing PUFAs measured in α-syn and ACSL4 KD LUHMES cells.

*(legend continued on next page)*

In search of potential mechanisms that underlie the observed evasion from ferroptosis in the α-syn-depleted neurons, PL membrane composition in the α-syn KD neurons was measured by mass spectrometry and compared with the effects caused by a reduction in ACSL4 expression. Similar to previous reports in other cell types (Doll et al., 2017), the percentages of total phosphatidylcholine- and phosphatidylethanolamine-containing PUFAs (PC PUFAs or PE PUFAs, respectively) were reduced in the ACSL4-depleted dopaminergic neurons (Figure 4A). A similar profile was observed when α-syn levels were reduced (Figure 4A), with no significant changes to MUFA content (Figure S4), indicating that α-syn may mediate the PL PUFA content in dopaminergic neurons through a similar pathway as ACSL4. To elucidate how these changes in PC and PE would impact on the generation of lipid peroxides, an index of peroxidability (PI) (Naudí et al., 2017) was calculated for each condition (PI = (% monoenoic FA × 0.025) + (% dienoic FA × 1) + (% trienoic FA × 2) + (% tetraenoic FA × 4) + (% pentaenoic FA × 6) + (% hexaenoic FA × 8). This index, which takes into account the number of double bonds in the PUFAs to determine the risk of PLs to oxidize, was reduced in LUHMES neurons with either α-syn or ACSL4 depleted by siRNA (Figure 4B).

Taking more in-depth lipidomic profiling of the different PC and PE molecular species in neurons with either α-syn or ACSL4 depleted revealed a prominent and selective loss of ether-PLs (highlighted in Figure 4C). Unlike ester-linked diacyl-PLs, ether-PLs possesses an ether bond at the glycerol sn-1 position. Ether-PLs comprise of two subclasses: alkyl-ether phospholipids (ePLs) and vinyl-ether phospholipids, also known as plasmalogens (pPLs). In the sn-2 position, ether-PLs most often contain a PUFA, which is prone to peroxidation. Finally, in the sn-3 position, ether-PLs present a polar head group, commonly a phosphoethanolamine and phosphocholine (Figures 4D and 4E). Of note, recent studies have shown that ether-PLs are essential for ferroptosis and that a reduction in ether-PLs suffices to protect cells against this unique cell-death pathway (Zou et al., 2020; Cui et al., 2021). In line with these findings, reduced α-syn or ACSL4 expression in LUHMES cells resulted in a specific downregulation of ether-linked PC (ether-PC) and PE (ether-PE) (Figures 4C and 4F). Upon evaluating specific ether-PL species previously associated with an increased vulnerability to ferroptosis (Cui et al., 2021), several were observed to be consistently downregulated in LUHMES dopaminergic neurons where α-syn or ACSL4 was depleted (Figures S5A and S5B). Taken together, these findings indicate that a key factor in α-syn's capability to mediate the sensitivity of dopaminergic neurons to ferroptosis-induced lipid peroxidation and cell death is through ether-PL modulation in the plasma membrane.

## The level of ether-PL in α-syn-depleted neurons is restored upon AA treatment

A reduction in ether-PLs upon α-syn depletion could be explained by (1) greater peroxidation of the PUFAs within the ether-PLs, (2) increased removal from the plasma membrane by the relevant phospholipase, and/or (3) impaired biosynthesis. The loss of all molecular species of ether-PLs, regardless of FA length or saturation status (Figure 4C), indicates an unlikelihood that reduced α-syn caused greater peroxidation of the PUFA in the ether-PLs, and thus this avenue of investigation was not pursued further. The calcium-independent phospholipase A2 (iPLA2) has been implicated in the removal of ether-PLs from the plasma membrane (Wolf and Gross, 1985; Ford et al., 1991; Yang et al., 1996). However, a lack of change to iPLA2 in the α-syn-depleted neurons makes increased enzymatic removal of ether-PLs from the plasma membrane also an unlikely protective mechanism (Figure 5A).

To assess whether the observed downregulation of ether-PLs in the α-syn KD cells might be driven by defective biogenesis at the peroxisome, established peroxisome markers (peroxisomal biogenesis factors 3 and 14 [PEX3 and PEX14, respectively]) were assessed along with the enzymes (fatty acyl-CoA reductase 1 [FAR1], glyceronephosphate O-acyltransferase [GNPAT], alkyldihydroxyacetonephosphate synthase [AGPS], and 1-acylglycerol-3-phosphate O-acyltransferase 3 [AGPAT3]) required for the synthesis of the ether-PL precursor 1-*O*-alkyl-glycerol-3-phosphate (AGP) (Figures 5A–5C). Again, similar to ACSL4 KD, neither levels of peroxisome markers or the relevant upstream proteins required for ether-PL biogenesis were altered (Figures 5A and 5B), suggesting that the initial stages of ether-PL synthesis were not impaired.

The role of ACSL4 is essential for the generation and incorporation of PUFA-CoA into the ferroptosis-relevant ether-PL in the ER (Figure 5C). Supplementation of AA (20 μM), the preferential substrate of ACSL4, restored ether-PLs back to control levels in LUHMES depleted of ACSL4 (Figures 5D and 5E). Similarly, AA supplementation restored the levels of ether-PLs upon a-syn depletion (Figures 5D and 5E) despite no observable changes in ACSL4 expression (Figures 5A, S1A, and S1B), suggesting that the changes in ether-PLs may be due to a lack of the PUFA-CoA required for ether-PL synthesis.

These results provide evidence to support a requirement for ether-PL in ferroptotic cell death not only in cancer cells (Zou et al., 2020; Cui et al., 2021) but also dopaminergic neurons, which have a greater amount of PUFA-containing ether-PLs (PUFA-ether-PLs) than PUFA-containing diacyl PLs (PUFA-diacyl-PLs) (Figures S6A and S6B). Furthermore, α-syn appears to play a critical role in ferroptosis sensitivity in dopaminergic

(C) Heatmaps comparing the abundance of the different PC and PE molecular species in α-syn and ACSL4 KD LUHMES cells relative to Ctrl KD. Highlighted in yellow are ether-linked phospholipids shown to be reduced in both the α-syn and ACSL4 KD conditions.
(D) Schematic representation of the distinct structures of diacyl phospholipids and the two subtypes of ether-linked phospholipids.
(E) The chemical structure of an example alkyl-ether PL, PE (16:0e/20:4), and a plasmalogen, PE (16:0p/20:4).
(F) Volcano plots of the expression changes to the phospholipids, with each subtype grouped by color, for α-syn versus Ctrl KD (left) and ACSL4 versus Ctrl KD (right) LUHMES cells.
Data represent mean of six replicates. Statistical mean comparisons in (A) and (B) were made using the unpaired one-tailed Student's t test (*$p < 0.05$), and data in (C) are represented as a $\log_2$ fold change.

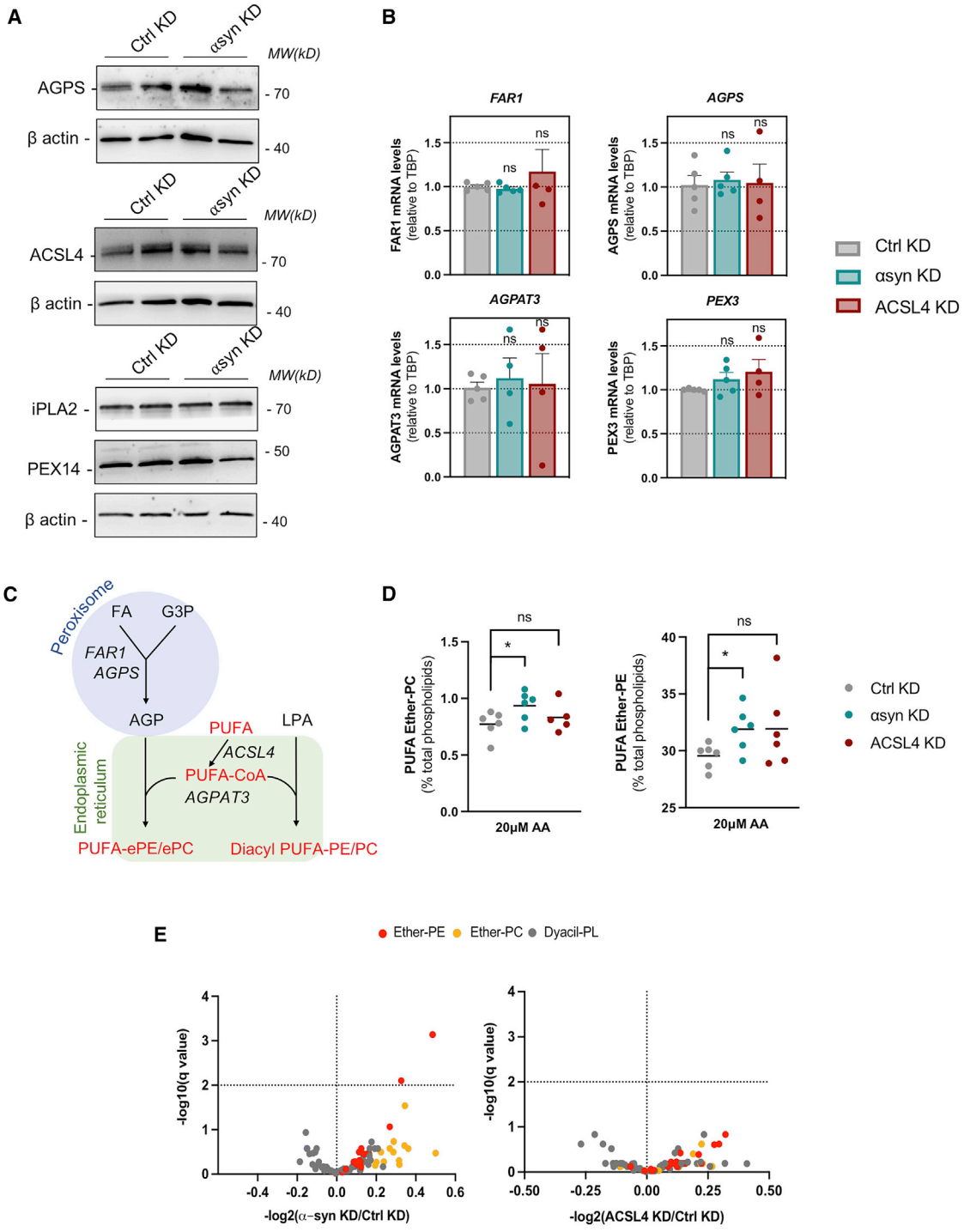


**Figure 5. AA treatment restores ether-PL levels in neurons that have a depletion in α-syn or ACSL4**

(A and B) Protein (A) and mRNA (B) expression of several key enzymes involved in the ether-PL biosynthesis pathway in α-syn and ACSL4 KD LUHMES. The relative gene expression was normalized to TBP.

(C) Schematic representation of the ether-PL biosynthesis pathway starting at the peroxisomal level through to the ER. FA, fatty acid; LPA, lysophosphatidic acid; G3P, glycerol-3-phosphate.

(D) PUFA-ether-PC and PUFA-ether-PE proportion measured in α-syn and ACSL4 after AA (20 μM; 24 h) supplementation.

(E) Volcano plots illustrating changes in the neuronal PE and PC phospholipid composition upon KD of α-syn or ACSL4 and treatment with AA (20 μM; 24 h).

Data represent the mean ± SEM from three independent experiments. Statistical mean comparisons in (B) and (D) were made using the unpaired two-tailed Student's t test (*$p < 0.05$).

neurons through modulation of ether-PL synthesis, strengthening a mechanistic link between endogenous α-syn and ferroptosis in neurons.

## DISCUSSION

Ferroptosis has been established as a regulated cell-death pathway with implications in several diseases (Friedmann Angeli et al., 2014; Linkermann et al., 2014; Do Van et al., 2016; Martin-Sanchez et al., 2017; Zhang et al., 2018b; Alim et al., 2019). Although the precise molecular pathways associated with ferroptosis continue to expand and evolve, extensive research to date has deciphered several key regulatory mechanisms. Here, we reveal that α-syn mediates the sensitivity of dopaminergic neurons to ferroptosis by enriching cellular membranes with ether-PLs. These findings further implicate ferroptosis in PD, which is supported by prior studies that reveal changes in PD consistent with ferroptosis, including iron overload (Dexter et al., 1987, 1989a; Hirsch et al., 1991; Ayton et al., 2015), elevated lipid peroxidation (Dexter et al., 1986, 1989b; de Farias et al., 2016), reduced glutathione (GSH) levels (Sofic et al., 1992; Sian et al., 1994; Pearce et al., 1997; Li et al., 1997), XcT downregulation (Vallerga et al., 2020), and CoQ10 reduction (Battino et al., 1996; Mischley et al., 2012; Bersuker et al., 2019). The potential role of ferroptosis in PD pathology is further strengthened by the recent finding that DJ-1, a gene linked to autosomal-recessive early-onset PD (Bonifati et al., 2003), acts as a ferroptosis inhibitor by preserving the transsulfuration pathway and thereby the biosynthesis of cysteine and GSH (Cao et al., 2020). Furthermore, a recent analysis associated DNA hypermethylation in the promotor region of the SLC7A11 gene (encoding the cysteine-glutamate antiporter XcT) to risk of PD. This hypermethylation of SLC7A11 results in a downregulation of XcT, which contributes to the decreased intracellular GSH levels observed in PD and the increased susceptibility to ferroptosis (Vallerga et al., 2020). Together, these well-established disease features strongly implicate ferroptosis in the neurodegeneration observed in PD. To this extent, we have previously shown that ferroptosis is a prevalent cell-death pathway in several oxidative stress models of Parkinsonism (Do Van et al., 2016). Despite this growing evidence, the implication as to whether ferroptosis is present in synucleinopathy models remains less clear. The recent findings that exogenous α-syn oligomers bind the plasma membrane to drive ferroptotic cell death through lipid peroxide generation, and that this can be rescued by iron chelators, D-PUFAs, or ferrostatin-1, provide the first evidence to support ferroptosis as a pathological mechanisms in synucleinopathies (Angelova et al., 2020). However, our study now goes further in implicating endogenous α-syn in the ferroptosis pathway by demonstrating that cellular α-syn expression can modulate the sensitivity of dopaminergic neurons to ferroptotic cell death in a similar way to the pro-ferroptotic enzyme ACSL4. Using two relevant human dopaminergic neuron *in vitro* models, we show that a reduction in α-syn expression protects neurons from ferroptosis-induced lipid peroxidation accumulation and subsequent cell death. Of relevance, human smNPC-derived midbrain neurons carrying a familial PD multiplication in *SNCA* (*SNCA* Trip) that results in elevated levels of α-syn has an opposing effect: increasing the vulnerability of neurons to ferroptosis-induced lipid peroxidation and cell death. An elevated basal lipid peroxidation in these *SNCA* Trip neurons supports similar observations in lipid ROS levels in *SNCA* Trip induced pluripotent stem cell (iPSC)-derived cortical neurons (Angelova et al., 2020) and suggests a residual priming effect that increases ferroptosis susceptibility in synucleinopathy conditions where there is an imbalance in redox homeostasis. Indeed, elevated oxidative stress and, more specifically, lipid peroxidation markers, including the metabolite 4-hydroxy-2-nonenal (4-HNE), are conspicuous features of sporadic PD pathology (Dexter et al., 1986; Di Domenico et al., 2017). In this study, α-syn was shown to determine the sensitivity of neurons to ferroptosis cell death, while no effect was observed against apoptosis, suggesting a ferroptosis-specific effect. However, the implication of α-syn in other cell-death mechanisms such as pyroptosis, parthanatos, or necroptosis remains unanswered and provides a prospect for future research.

The role of ether-PLs in health and disease has gained increasing attention, especially since they were recently shown to drive ferroptosis in cancer cells (Zou et al., 2020; Cui et al., 2021). Recent studies have shown that depletion of ether-PL biosynthesis enzymes (GNPAT, FAR1, AGPS, and AGPAT3) decreases the level of PUFA-ether-PLs and markedly promotes ferroptosis resistance, while supplementation of PUFA-ether-PLs in cells with deficiency in ether-PL synthesis resensitize these cells to ferroptosis (Zou et al., 2020). Of note, supplementing cells with either PUFA-ether-PLs or their non-ePL counterparts has a similar sensitizing effect on ferroptosis suggesting that PUFA-ether-PLs are not intrinsically more sensitive to peroxidation than other PUFA-PLs. However, ether-PLs are essential in driving ferroptosis, perhaps because they represent an abundant pool of PUFA-PLs that are available for peroxidation. This is particularly relevant in neurons, as the brain has the highest proportion of ether-PLs, more specifically ether-Pes, which represent >50% of total PE (Brites et al., 2004). In line with this, SH-SY5Y neuroblastoma cells acquire sensitivity to ferroptosis as the levels of ether-PLs increase during differentiation (Zou et al., 2020). Furthermore, the observation that LUHMES dopaminergic neurons have a greater proportion of PUFA-ether-PE than PUFA-dyacil-PE (Figures S6A and S6B) suggests that ferroptosis unfolding in neurons may be governed by peroxidation of ether-PLs. Here, we describe the importance in α-syn modulation of ether-PL membrane composition to regulate ferroptosis sensitivity in dopaminergic neurons. Similar to ACSL4, this function of α-syn is not related to the upstream enzymes involved with the early stages of biosynthesis at the peroxisome or an abnormal removal from the plasma membrane via iPLA2 since no alteration in protein or mRNA levels was detected. However, a modulation of the enzymatic activity of such enzymes cannot be excluded. The restoration of ether-PL levels by AA in neurons depleted of α-syn paralleled that observed with ACSL4 depletion and suggests an impaired activity of ACSL4 in dopaminergic neurons lacking α-syn. This hypothesis is strengthened by Golovko and colleagues, who reported a reduction in AA-CoA mass and AA incorporation into PLs in the brains of *SNCA* KO mice due to a reduction in total ACSL activity (Golovko et al., 2006). This ACSL activity was restored upon

addition of exogenous α-syn, indicating a role of α-syn in the control of ACSL4 in AA-CoA formation. Furthermore, we now also strengthen a link between α-syn and ether-PLs that was previously reported in brains of a synucleinopathy mouse model (A53T α-syn) with higher levels of plasmalogens, specifically derivates of either C16:0 or C18:0 (Yakunin et al., 2014).

α-Synuclein has a high degree of sequence homology with apolipoproteins (Eichmann et al., 2017; Fecchio et al., 2018), is implicated in the metabolism of lipids (most prevalently membrane PUFAs including AA, adrenic acid, linoleic acid, and dihomo-gamma-linoleic acid) (Sharon et al., 2003; Golovko et al., 2006; Barceló-Coblijn et al., 2007), and has a high binding affinity to PUFAs (α-linolenic acid, DHA, and eicosapentaenoic acid) through its N-terminal domain. Both the lipid ratio of these PUFAs in the plasma membrane and the membrane fluidity are increased when α-syn levels are elevated both in neuronal cultures and brain tissue from patients with PD and DLB (Sharon et al., 2003). Conversely, when exposed to free or PL-bound PUFAs, α-syn undergoes structural changes including an increased propensity to oligomerize (Sharon et al., 2001; Broersen et al., 2006; De Franceschi et al., 2009). Direct or indirect enrichment of cellular membranes with diacyl- and ether-PLs containing PUFAs by α-syn under the PD pathological conditions of elevated free labile iron and oxidative stress may lead to further lipid peroxidation and drive neurons toward ferroptotic cell death. In addition to the already mentioned associations between α-syn and the metabolism of PUFAs, interactions between α-syn and iron have also been extensively reported (reviewed in Mahoney-Sánchez et al., 2020). These include alterations in transferrin receptor-mediated iron import when α-syn is depleted (Baksi et al., 2016) and impaired ferritinophagy upon α-syn overexpression (Baksi and Singh, 2017).

The implicated role of endogenous α-syn with the metabolism of ether-PLs provides a direct link to an established pathway involved in lipid peroxidation that is essential for ferroptosis. These observations also reveal a cell-death mechanism in dopaminergic neurons from patients where α-syn levels are dysregulated, including synucleinopathies such as PD. This provides further support to that already presented (Sofic et al., 1992; Sian et al., 1994; Pearce et al., 1997; Li et al., 1997; Devos et al., 2014; Vallerga et al., 2020; Bonifati et al., 2003; Cao et al., 2020; Battino et al., 1996; Mischley et al., 2012; Bersuker et al., 2019) for targeting ferroptosis as a therapeutic strategy in synucleinopathies.

### Limitations of the study

One limitation of our work is that when studying the implication of α-syn in ferroptosis, α-syn was not fully removed from LUHMES cells. As shown in Figures 1 and 2, ferroptosis sensitivity was measured in α-syn KD and 140 α-syn KO LUHMES cells, where α-syn expression level is transiently reduced by siRNA or the main 140-aa-long isoform deleted by CRISPR-Cas9, respectively. However, the expression of β- and γ-syn, and the shorter α-syn isoforms generated by alternative splicing, were not measured and characterized in LUHMES cells. Furthermore, although a link between α-syn expression and ferroptosis sensitivity was provided in two dopaminergic cell lines (LUHMES and smNPC-derived mDANs), the plasma membrane composition was only analyzed in α-syn and ACSL4 KD LUHMES cells. Lipidomic analyses in smNPC-derived mDANS are required to confirm whether α-syn modulation of the ether-PL composition also occurs when α-syn expression is elevated. In addition, why depletion of α-syn results in a reduced ether-PL content in the plasma membrane remains unclear, and further functional studies are required to decipher how α-syn regulates the plasma membrane PL composition. Finally, while necessary for mechanistic studies, all experimentation was conducted in single-cell models. *Ex vivo* or *in vivo* follow-up studies will be important to confirm that these data are physiologically relevant in a multicellular environment such as the brain.

## STAR★METHODS

Detailed methods are provided in the online version of this paper and include the following:

- KEY RESOURCES TABLE
- RESOURCE AVAILABILITY
  - Lead contact
  - Materials availability
  - Data and code availability
- EXPERIMENTAL MODEL AND SUBJECT DETAILS
  - Cell lines
- METHOD DETAILS
  - Cell culture
  - Quantification and statistical analysis

### SUPPLEMENTAL INFORMATION

Supplemental information can be found online at https://doi.org/10.1016/j.celrep.2022.111231.

### ACKNOWLEDGMENTS

The authors wish to thank the BioImaging Center Lille (BiCel) platform, and in particular Nathalie Jouy, for the support given in the flow cytometry experiments. The authors wish to thank the support of the Lille University Hospital and NS-Park/FCRIN clinical research network, the European commission for grant no. 633190 of the H2020 program, NCT02655315. This work was supported in part by European funds Network of Centres of Excellence in Neurodegeneration (CoEN) PRION-IRON and European funds (H2020, Eurostar) for preclinical research E-PD-IRONSYN. The work of I.B. and R.K. was supported by grants from Luxembourg National Research Fund (FNR) for the PEARL program (FNR/P13/6682797 to R.K.), MotaSYN (12719684), and MAMasyn.

### AUTHOR CONTRIBUTIONS

Conceptualization, D.D., J.-C.D., L.M.-S., and J.A.D; methodology, A.J., K.T., L.M.-S., and J.-C.D.; investigation, L.M.-S., I.D., and H.B.; formal analysis, O.B.; writing – original draft, L.M.-S.; writing – review & editing, J.A.D., D.D., R.K., and S.A.; supervision, J.A.D., D.D., and J.-C.D.; funding acquisition, D.D. and R.K.

### DECLARATION OF INTERESTS

D.D. has received PHRC grants from the French Ministry of Health and research funding from the ARSLA charity, France Parkinson charity, and the Credit Agricole Foundation. He has led two pilot investigator-driven studies with DFP provided for free by ApoPharma (FAIRPARK-I and SAFE-FAIR ALS-I). He is leading two large investigator-driven studies with DFP provided

for free by ApoPharma (FAIRPARK-II and FAIR ALS-II). He served on advisory boards, served as a consultant, and has given lectures for pharmaceutical companies such as Orkyn, Aguettant, Abbvie, Medtronic, Novartis, Teva, UCB, and Lundbeck. J.A.D. has received research funding from Alzheimer's Society, Alzheimer's Research UK, European Commission, Parkinson's UK, and NHMRC. He serves as a scientific advisor on the FAIR-PARK II but has no financial disclosures. The remaining authors have nothing to declare.

Received: April 21, 2022
Revised: June 15, 2022
Accepted: July 27, 2022
Published: August 16, 2022

## REFERENCES

Alim, I., Caulfield, J.T., Chen, Y., Swarup, V., Geschwind, D.H., Ivanova, E., Seravalli, J., Ai, Y., Sansing, L.H., Ste Marie, E.J., et al. (2019). Selenium drives a transcriptional adaptive program to block ferroptosis and treat stroke. Cell *177*, 1262–1279.e25. https://doi.org/10.1016/j.cell.2019.03.032.

Angelova, P.R., Choi, M.L., Berezhnov, A.V., Horrocks, M.H., Hughes, C.D., De, S., Rodrigues, M., Yapom, R., Little, D., Dolt, K.S., et al. (2020). Alpha synuclein aggregation drives ferroptosis: an interplay of iron, calcium and lipid peroxidation. Cell Death Differ. *27*, 2781–2796. https://doi.org/10.1038/s41418-020-0542-z.

Ayton, S., Lei, P., Hare, D.J., Duce, J.A., George, J.L., Adlard, P.A., McLean, C., Rogers, J.T., Cherny, R.A., Finkelstein, D.I., and Bush, A.I. (2015). Parkinson's disease iron deposition caused by nitric oxide-induced loss of β-amyloid precursor protein. J. Neurosci. *35*, 3591–3597. https://doi.org/10.1523/JNEUROSCI.3439-14.2015.

Baksi, S., and Singh, N. (2017). α-Synuclein impairs ferritinophagy in the retinal pigment epithelium: implications for retinal iron dyshomeostasis in Parkinson's disease. Sci. Rep. *7*, 12843. https://doi.org/10.1038/s41598-017-12862-x.

Baksi, S., Tripathi, A.K., and Singh, N. (2016). Alpha-synuclein modulates retinal iron homeostasis by facilitating the uptake of transferrin-bound iron: implications for visual manifestations of Parkinson's disease. Free Radic. Biol. Med. *97*, 292–306. https://doi.org/10.1016/j.freeradbiomed.2016.06.025.

Barbuti, P., Antony, P., Santos, B., Massart, F., Cruciani, G., Dording, C., Arias, J., Schwamborn, J., and Krüger, R. (2020a). Using high-content screening to generate single-cell gene-corrected patient-derived iPS clones reveals excess alpha-synuclein with familial Parkinson's disease point mutation A30P. Cells *9*, 2065. https://doi.org/10.3390/cells9092065.

Barbuti, P.A., Santos, B.F.R., Dording, C.M., Cruciani, G., Massart, F., Hummel, A., and Krüger, R. (2020b). Generation of two iPS cell lines (HIHDNDi001-A and HIHDNDi001-B) from a Parkinson's disease patient carrying the heterozygous p.A30P mutation in SNCA. Stem Cell Res. *48*, 101951. https://doi.org/10.1016/j.scr.2020.101951.

Barceló-Coblijn, G., Golovko, M.Y., Weinhofer, I., Berger, J., and Murphy, E.J. (2007). Brain neutral lipids mass is increased in alpha-synuclein gene-ablated mice. J. Neurochem. *101*, 132–141. https://doi.org/10.1111/j.1471-4159.2006.04348.x.

Battino, M., Littarru, G.P., Gorini, A., and Villa, R.F. (1996). Coenzyme Q, peroxidation and cytochrome oxidase features after Parkinson's-like disease by MPTP toxicity in intra-synaptic and non-synaptic mitochondria from Macaca fascicularis cerebral cortex and hippocampus: action of dihydroergocriptine. Neurochem. Res. *21*, 1505–1514. https://doi.org/10.1007/BF02533098.

Bersuker, K., Hendricks, J.M., Li, Z., Magtanong, L., Ford, B., Tang, P.H., Roberts, M.A., Tong, B., Maimone, T.J., Zoncu, R., et al. (2019). The CoQ oxidoreductase FSP1 acts parallel to GPX4 to inhibit ferroptosis. Nature *575*, 688–692. https://doi.org/10.1038/s41586-019-1705-2.

Blauwendraat, C., Heilbron, K., Vallerga, C.L., Bandres-Ciga, S., von Coelln, R., Pihlstrøm, L., Simón-Sánchez, J., Schulte, C., Sharma, M., Krohn, L., et al. (2019). Parkinson's disease age at onset genome-wide association study: defining heritability, genetic loci, and α-synuclein mechanisms. Mov. Disord. *34*, 866–875. https://doi.org/10.1002/mds.27659.

Bonifati, V., Rizzu, P., van Baren, M.J., Schaap, O., Breedveld, G.J., Krieger, E., Dekker, M.C.J., Squitieri, F., Ibanez, P., Joosse, M., et al. (2003). Mutations in the DJ-1 gene associated with autosomal recessive early-onset parkinsonism. Science *299*, 256–259. https://doi.org/10.1126/science.1077209.

Boussaad, I., Obermaier, C.D., Hanss, Z., Bobbili, D.R., Bolognin, S., Glaab, E., Wołyńska, K., Weisschuh, N., De Conti, L., May, C., et al. (2020). A patient-based model of RNA mis-splicing uncovers treatment targets in Parkinson's disease. Sci. Transl. Med. *12*, eaau3960. https://doi.org/10.1126/scitranslmed.aau3960.

Brites, P., Waterham, H.R., and Wanders, R.J.A. (2004). Functions and biosynthesis of plasmalogens in health and disease. Biochim. Biophys. Acta *1636*, 219–231. https://doi.org/10.1016/j.bbalip.2003.12.010.

Broersen, K., van den Brink, D., Fraser, G., Goedert, M., and Davletov, B. (2006). Alpha-synuclein adopts an alpha-helical conformation in the presence of polyunsaturated fatty acids to hinder micelle formation. Biochemistry *45*, 15610–15616. https://doi.org/10.1021/bi061743l.

Cao, J., Chen, X., Jiang, L., Lu, B., Yuan, M., Zhu, D., Zhu, H., He, Q., Yang, B., and Ying, M. (2020). DJ-1 suppresses ferroptosis through preserving the activity of S-adenosyl homocysteine hydrolase. Nat. Commun. *11*, 1251. https://doi.org/10.1038/s41467-020-15109-y.

Cui, W., Liu, D., Gu, W., and Chu, B. (2021). Peroxisome-driven ether-linked phospholipids biosynthesis is essential for ferroptosis. Cell Death Differ. *28*, 2536–2551. https://doi.org/10.1038/s41418-021-00769-0.

de Farias, C.C., Maes, M., Bonifácio, K.L., Bortolasci, C.C., de Souza Nogueira, A., Brinholi, F.F., Matsumoto, A.K., do Nascimento, M.A., de Melo, L.B., Nixdorf, S.L., et al. (2016). Highly specific changes in antioxidant levels and lipid peroxidation in Parkinson's disease and its progression: disease and staging biomarkers and new drug targets. Neurosci. Lett. *617*, 66–71. https://doi.org/10.1016/j.neulet.2016.02.011.

De Franceschi, G., Frare, E., Bubacco, L., Mammi, S., Fontana, A., and de Laureto, P.P. (2009). Molecular insights into the interaction between alpha-synuclein and docosahexaenoic acid. J. Mol. Biol. *394*, 94–107. https://doi.org/10.1016/j.jmb.2009.09.008.

Devos, D., Moreau, C., Devedjian, J.C., Kluza, J., Petrault, M., Laloux, C., Jonneaux, A., Ryckewaert, G., Garçon, G., Rouaix, N., et al. (2014). Targeting chelatable iron as a therapeutic modality in Parkinson's disease. Antioxid. Redox Signal. *21*, 195–210. https://doi.org/10.1089/ars.2013.5593.

Devos, D., Moreau, C., Kyheng, M., Garçon, G., Rolland, A.S., Blasco, H., Gelé, P., Timothée Lenglet, T., Veyrat-Durebex, C., Corcia, P., et al. (2019). A ferroptosis–based panel of prognostic biomarkers for Amyotrophic Lateral Sclerosis. Sci. Rep. *9*, 2918–2926. https://doi.org/10.1038/s41598-019-39739-5.

Dexter, D., Carter, C., Agid, F., Agid, Y., Lees, A.J., Jenner, P., and Marsden, C.D. (1986). Lipid peroxidation as cause of nigral cell death in Parkinson's disease. Lancet *2*, 639–640. https://doi.org/10.1016/s0140-6736(86)92471-2.

Dexter, D.T., Wells, F.R., Agid, F., Agid, Y., Lees, A.J., Jenner, P., and Marsden, C.D. (1987). Increased nigral iron content in postmortem parkinsonian brain. Lancet *2*, 1219–1220. https://doi.org/10.1016/s0140-6736(87)91361-4.

Dexter, D.T., Wells, F.R., Lees, A.J., Agid, F., Agid, Y., Jenner, P., and Marsden, C.D. (1989a). Increased nigral iron content and alterations in other metal ions occurring in brain in Parkinson's disease. J. Neurochem. *52*, 1830–1836. https://doi.org/10.1111/j.1471-4159.1989.tb07264.x.

Dexter, D.T., Carter, C.J., Wells, F.R., Javoy-Agid, F., Agid, Y., Lees, A., Jenner, P., and Marsden, C.D. (1989b). Basal lipid peroxidation in substantia nigra is increased in Parkinson's disease. J. Neurochem. *52*, 381–389. https://doi.org/10.1111/j.1471-4159.1989.tb09133.x.

Di Domenico, F., Tramutola, A., and Butterfield, D.A. (2017). Role of 4-hydroxy-2-nonenal (HNE) in the pathogenesis of alzheimer disease and other selected age-related neurodegenerative disorders. Free Radic. Biol. Med. *111*, 253–261. https://doi.org/10.1016/j.freeradbiomed.2016.10.490.

Dixon, S.J., Lemberg, K.M., Lamprecht, M.R., Skouta, R., Zaitsev, E.M., Gleason, C.E., Patel, D.N., Bauer, A.J., Cantley, A.M., Yang, W.S., et al.

(2012). Ferroptosis: an iron-dependent form of nonapoptotic cell death. Cell *149*, 1060–1072. https://doi.org/10.1016/j.cell.2012.03.042.

Do Van, B., Gouel, F., Jonneaux, A., Timmerman, K., Gelé, P., Pétrault, M., Bastide, M., Laloux, C., Moreau, C., Bordet, R., et al. (2016). Ferroptosis, a newly characterized form of cell death in Parkinson's disease that is regulated by PKC. Neurobiol. Dis. *94*, 169–178. https://doi.org/10.1016/j.nbd.2016.05.011.

Doll, S., Proneth, B., Tyurina, Y.Y., Panzilius, E., Kobayashi, S., Ingold, I., Irmler, M., Beckers, J., Aichler, M., Walch, A., et al. (2017). ACSL4 dictates ferroptosis sensitivity by shaping cellular lipid composition. Nat. Chem. Biol. *13*, 91–98. https://doi.org/10.1038/nchembio.2239.

Eichmann, C., Kumari, P., and Riek, R. (2017). High-density lipoprotein-like particle formation of Synuclein variants. FEBS Lett. *591*, 304–311. https://doi.org/10.1002/1873-3468.12543.

Fecchio, C., Palazzi, L., and de Laureto, P.P. (2018). α-Synuclein and polyunsaturated fatty acids: molecular basis of the interaction and implication in neurodegeneration. Molecules *23*, E1531. https://doi.org/10.3390/molecules23071531.

Folch, J., Lees, M., and Sloane Stanley, G.H. (1957). A simple method for the isolation and purification of total lipides from animal tissues. J. Biol. Chem. *226*, 497–509.

Ford, D.A., Hazen, S.L., Saffitz, J.E., and Gross, R.W. (1991). The rapid and reversible activation of a calcium-independent plasmalogen-selective phospholipase A2 during myocardial ischemia. J. Clin. Invest. *88*, 331–335. https://doi.org/10.1172/JCI115296.

Friedmann Angeli, J.P., Schneider, M., Proneth, B., Tyurina, Y.Y., Tyurin, V.A., Hammond, V.J., Herbach, N., Aichler, M., Walch, A., Eggenhofer, E., et al. (2014). Inactivation of the ferroptosis regulator Gpx4 triggers acute renal failure in mice. Nat. Cell Biol. *16*, 1180–1191. https://doi.org/10.1038/ncb3064.

Galluzzi, L., Vitale, I., Aaronson, S.A., Abrams, J.M., Adam, D., Agostinis, P., Alnemri, E.S., Altucci, L., Amelio, I., Andrews, D.W., et al. (2018). Molecular mechanisms of cell death: recommendations of the nomenclature committee on cell death 2018. Cell Death Differ. *25*, 486–541. https://doi.org/10.1038/s41418-017-0012-4.

Golovko, M.Y., Faergeman, N.J., Cole, N.B., Castagnet, P.I., Nussbaum, R.L., and Murphy, E.J. (2005). Alpha-synuclein gene deletion decreases brain palmitate uptake and alters the palmitate metabolism in the absence of alpha-synuclein palmitate binding. Biochemistry *44*, 8251–8259. https://doi.org/10.1021/bi0502137.

Golovko, M.Y., Rosenberger, T.A., Faergeman, N.J., Feddersen, S., Cole, N.B., Pribill, I., Berger, J., Nussbaum, R.L., and Murphy, E.J. (2006). Acyl-CoA synthetase activity links wild-type but not mutant alpha-synuclein to brain arachidonate metabolism. Biochemistry *45*, 6956–6966. https://doi.org/10.1021/bi0600289.

Golovko, M.Y., Rosenberger, T.A., Feddersen, S., Faergeman, N.J., and Murphy, E.J. (2007). Alpha-synuclein gene ablation increases docosahexaenoic acid incorporation and turnover in brain phospholipids. J. Neurochem. *101*, 201–211. https://doi.org/10.1111/j.1471-4159.2006.04357.x.

Guiney, S.J., Adlard, P.A., Bush, A.I., Finkelstein, D.I., and Ayton, S. (2017). Ferroptosis and cell death mechanisms in Parkinson's disease. Neurochem. Int. *104*, 34–48. https://doi.org/10.1016/j.neuint.2017.01.004.

Hirsch, E.C., Brandel, J.P., Galle, P., Javoy-Agid, F., and Agid, Y. (1991). Iron and aluminum increase in the substantia nigra of patients with Parkinson's disease: an X-ray microanalysis. J. Neurochem. *56*, 446–451. https://doi.org/10.1111/j.1471-4159.1991.tb08170.x.

Karuppagounder, S.S., Alin, L., Chen, Y., Brand, D., Bourassa, M.W., Dietrich, K., Wilkinson, C.M., Nadeau, C.A., Kumar, A., Perry, S., et al. (2018). N-acetylcysteine targets 5 lipoxygenase-derived, toxic lipids and can synergize with prostaglandin E2 to inhibit ferroptosis and improve outcomes following hemorrhagic stroke in mice. Ann. Neurol. *84*, 854–872. https://doi.org/10.1002/ana.25356.

Li, Y., Maher, P., and Schubert, D. (1997). A role for 12-lipoxygenase in nerve cell death caused by glutathione depletion. Neuron *19*, 453–463. https://doi.org/10.1016/s0896-6273(00)80953-8.

Linkermann, A., Skouta, R., Himmerkus, N., Mulay, S.R., Dewitz, C., De Zen, F., Prokai, A., Zuchtriegel, G., Krombach, F., Welz, P.-S., et al. (2014). Synchronized renal tubular cell death involves ferroptosis. Proc. Natl. Acad. Sci. USA *111*, 16836–16841. https://doi.org/10.1073/pnas.1415518111.

Magtanong, L., Ko, P.-J., To, M., Cao, J.Y., Forcina, G.C., Tarangelo, A., Ward, C.C., Cho, K., Patti, G.J., Nomura, D.K., et al. (2019). Exogenous monounsaturated fatty acids promote a ferroptosis-resistant cell state. Cell Chem. Biol. *26*, 420–432.e9. https://doi.org/10.1016/j.chembiol.2018.11.016.

Mahoney-Sánchez, L., Bouchaoui, H., Ayton, S., Devos, D., Duce, J.A., and Devedjian, J.-C. (2020). Ferroptosis and its potential role in the physiopathology of Parkinson's Disease. Prog. Neurobiol. *196*. https://doi.org/10.1016/j.pneurobio.2020.101890.

Martin-Sanchez, D., Ruiz-Andres, O., Poveda, J., Carrasco, S., Cannata-Ortiz, P., Sanchez-Niño, M.D., Ruiz Ortega, M., Egido, J., Linkermann, A., Ortiz, A., and Sanz, A.B. (2017). Ferroptosis, but not necroptosis, is important in nephrotoxic folic acid-induced AKI. J. Am. Soc. Nephrol. *28*, 218–229. https://doi.org/10.1681/ASN.2015121376.

Mischley, L.K., Allen, J., and Bradley, R. (2012). Coenzyme Q10 deficiency in patients with Parkinson's disease. J. Neurol. Sci. *318*, 72–75. https://doi.org/10.1016/j.jns.2012.03.023.

Mohamed, N.-V., Sirois, J., Ramamurthy, J., Mathur, M., Lépine, P., Deneault, E., Maussion, G., Nicouleau, M., Chen, C.X.-Q., Abdian, N., et al. (2021). Midbrain organoids with an SNCA gene triplication model key features of synucleinopathy. Brain Commun. *3*, fcab223. https://doi.org/10.1093/braincomms/fcab223.

Moreau, C., Duce, J.A., Rascol, O., Devedjian, J.-C., Berg, D., Dexter, D., Cabantchik, Z.I., Bush, A.I., and Devos, D.; FAIRPARK-II study group (2018). Iron as a therapeutic target for Parkinson's disease. Mov. Disord. *33*, 568–574. https://doi.org/10.1002/mds.27275.

Naudí, A., Cabré, R., Dominguez-Gonzalez, M., Ayala, V., Jové, M., Mota-Martorell, N., Piñol-Ripoll, G., Gil-Villar, M.P., Rué, M., Portero-Otín, M., et al. (2017). Region-specific vulnerability to lipid peroxidation and evidence of neuronal mechanisms for polyunsaturated fatty acid biosynthesis in the healthy adult human central nervous system. Biochim. Biophys. Acta. Mol. Cell Biol. Lipids, 485–495. https://doi.org/10.1016/j.bbalip.2017.02.001.

Pearce, R.K., Owen, A., Daniel, S., Jenner, P., and Marsden, C.D. (1997). Alterations in the distribution of glutathione in the substantia nigra in Parkinson's disease. J. Neural. Transm. *104*, 661–677. https://doi.org/10.1007/BF01291884.

Schneider, S.A., and Obeso, J.A. (2015). Clinical and pathological features of Parkinson's disease. Curr. Top. Behav. Neurosci. *22*, 205–220. https://doi.org/10.1007/7854_2014_317.

Sharon, R., Goldberg, M.S., Bar-Josef, I., Betensky, R.A., Shen, J., and Selkoe, D.J. (2001). alpha-Synuclein occurs in lipid-rich high molecular weight complexes, binds fatty acids, and shows homology to the fatty acid-binding proteins. Proc. Natl. Acad. Sci. USA *98*, 9110–9115. https://doi.org/10.1073/pnas.171300598.

Sharon, R., Bar-Joseph, I., Mirick, G.E., Serhan, C.N., and Selkoe, D.J. (2003). Altered fatty acid composition of dopaminergic neurons expressing alpha-synuclein and human brains with alpha-synucleinopathies. J. Biol. Chem. *278*, 49874–49881. https://doi.org/10.1074/jbc.M309127200.

Sian, J., Dexter, D.T., Lees, A.J., Daniel, S., Agid, Y., Javoy-Agid, F., Jenner, P., and Marsden, C.D. (1994). Alterations in glutathione levels in Parkinson's disease and other neurodegenerative disorders affecting basal ganglia. Ann. Neurol. *36*, 348–355. https://doi.org/10.1002/ana.410360305.

Sofic, E., Lange, K.W., Jellinger, K., and Riederer, P. (1992). Reduced and oxidized glutathione in the substantia nigra of patients with Parkinson's disease. Neurosci. Lett. *142*, 128–130. https://doi.org/10.1016/0304-3940(92)90355-b.

Spillantini, M.G., Schmidt, M.L., Lee, V.M., Trojanowski, J.Q., Jakes, R., and Goedert, M. (1997). Alpha-synuclein in Lewy bodies. Nature *388*, 839–840. https://doi.org/10.1038/42166.

Stockwell, B.R., Friedmann Angeli, J.P., Bayir, H., Bush, A.I., Conrad, M., Dixon, S.J., Fulda, S., Gascón, S., Hatzios, S.K., Kagan, V.E., et al. (2017). Ferroptosis: a regulated cell death nexus linking metabolism, redox biology, and disease. Cell *171*, 273–285. https://doi.org/10.1016/j.cell.2017.09.021.

Tang, D., Chen, X., Kang, R., and Kroemer, G. (2021). Ferroptosis: molecular mechanisms and health implications. Cell Res. *31*, 107–125. https://doi.org/10.1038/s41422-020-00441-1.

Vallerga, C.L., Zhang, F., Fowdar, J., McRae, A.F., Qi, T., Nabais, M.F., Zhang, Q., Kassam, I., Henders, A.K., Wallace, L., et al. (2020). Analysis of DNA methylation associates the cystine–glutamate antiporter SLC7A11 with risk of Parkinson's disease. Nat. Commun. *11*, 1238. https://doi.org/10.1038/s41467-020-15065-7.

Wolf, R.A., and Gross, R.W. (1985). Identification of neutral active phospholipase C which hydrolyzes choline glycerophospholipids and plasmalogen selective phospholipase A2 in canine myocardium. J. Biol. Chem. *260*, 7295–7303.

Yakunin, E., Kisos, H., Kulik, W., Grigoletto, J., Wanders, R.J.A., and Sharon, R. (2014). The regulation of catalase activity by PPAR $\gamma$ is affected by $\alpha$ -synuclein. Ann. Clin. Transl. Neurol. *1*, 145–159. https://doi.org/10.1002/acn3.38.

Yang, H.C., Farooqui, A.A., and Horrocks, L.A. (1996). Characterization of plasmalogen-selective phospholipase A2 from bovine brain. Adv. Exp. Med. Biol. *416*, 309–313. https://doi.org/10.1007/978-1-4899-0179-8_49.

Yang, W.S., Kim, K.J., Gaschler, M.M., Patel, M., Shchepinov, M.S., and Stockwell, B.R. (2016). Peroxidation of polyunsaturated fatty acids by lipoxygenases drives ferroptosis. Proc. Natl. Acad. Sci. USA *113*, E4966–E4975. https://doi.org/10.1073/pnas.1603244113.

Zhang, Y., Shu, L., Sun, Q., Pan, H., Guo, J., and Tang, B. (2018a). A comprehensive analysis of the association between SNCA polymorphisms and the risk of Parkinson's disease. Front. Mol. Neurosci. *11*, 391. https://doi.org/10.3389/fnmol.2018.00391.

Zhang, Z., Wu, Y., Yuan, S., Zhang, P., Zhang, J., Li, H., Li, X., Shen, H., Wang, Z., and Chen, G. (2018b). Glutathione peroxidase 4 participates in secondary brain injury through mediating ferroptosis in a rat model of intracerebral hemorrhage. Brain Res. *1701*, 112–125. https://doi.org/10.1016/j.brainres.2018.09.012.

Ziv, I., Shirvan, A., Offen, D., Barzilai, A., and Melamed, E. (2001). Molecular biology of dopamine-induced apoptosis : possible implications for Parkinson's disease. Methods Mol. Med. *62*, 73–87. https://doi.org/10.1385/1-59259-142-6:73.

Zou, Y., Henry, W.S., Ricq, E.L., Graham, E.T., Phadnis, V.V., Maretich, P., Paradkar, S., Boehnke, N., Deik, A.A., Reinhardt, F., et al. (2020). Plasticity of ether lipids promotes ferroptosis susceptibility and evasion. Nature *585*, 603–608. https://doi.org/10.1038/s41586-020-2732-8.

## STAR★METHODS

### KEY RESOURCES TABLE

| REAGENT or RESOURCE | SOURCE | IDENTIFIER |
|---|---|---|
| Antibodies | | |
| anti α-syn (MJFR1) | Abcam | Cat#ab138501; RRID:AB_2537217 |
| anti α-syn (4D6) | BioLegend | Cat# 834,303; RRID:AB_2564985 |
| anti ACSL4 (EPR8640) | Abcam | Cat#ab155282; RRID:AB_2714020 |
| anti PEX14 | Abcam | Cat#ab183885; RRID:AB_2744539 |
| anti AGPS | Abcam | Cat#ab236621; RRID:AB_2921211 |
| anti GNPAT | Proteintech | Cat#14931-1-AP; RRID:AB_2110546 |
| anti PLA2G6 | Proteintech | Cat#22030-1-AP; RRID:AB_2878976 |
| Chemicals, peptides, and recombinant proteins | | |
| Erastin | Sigma | Cat#E7781 |
| Staurosporin | Sigma | Cat#S4400 |
| N6, 2′-O-dibutyryl cAMP sodium (cAMP) | Sigma | Cat#D0627 |
| Tetacyclin | Sigma | Cat#T-7660 |
| Poly-L-Ornithune | Sigma | Cat#P3655 |
| Fibronectin | Sigma | Cat#F1141 |
| Arachidonic Acid | Sigma | Cat#10931 |
| RSL3 | Selleckhem | Cat#S8155 |
| N2 | Thermo Fisher Scientific | Cat#17502048 |
| Advanced DMEM/F12 | Thermo Fisher Scientific | Cat#12634-028 |
| Glutamine | Thermo Fisher Scientific | Cat#25030-123 |
| BODIPY 581/591 C11 | Thermo Fisher Scientific | Cat#D3861 |
| LIVE/DEAD Blue | Thermi Fisher Scientific | Cat#L23105 |
| Lipofectamine RNAiMAX | Thermo Fisher Scientific | Cat#13778150 |
| OptiMEM Reduced Serum Media | Thermo Fisher Scientific | Cat#10149832 |
| bGFG | R&D Systems | Cat#4114-TC |
| GDNF | R&D Systems | Cat#212-GT |
| Rho-Kinase inhibitor (Y-27632) | abcam | Cat#ab120129 |
| FGF8 | Peprotech | Cat#100-25 |
| BDNF | Peprotech | Cat#450-02 |
| TGF-β3 | Peprotech | Cat#100-36E |
| Critical commercial assays | | |
| Pierce BCA protein assay kit | Thermo Fisher Scientific | Cat#23225 |
| Deposited data | | |
| Raw and analyzed phospholipid measurements | This paper | Mendeley Data: https://doi.org/10.17632/dh9hjpsz7t.1 |
| Experimental models: Cell lines | | |
| LUHMES Cell line | Kind gift from Pr. Marcel Leist (University of Konstanz) | Developed by J Lotharius 1998 |
| iPSC SNCA Tiplication cell line | EBISC | Edi001-A |
| 140 α-syn KO LUHMES cell lines | This paper | N/A |
| iPSC isogenic control | Mohamed et al. (2021) | Developed and kindly provided by Dr. Tilo Kunath from the University of Edinburg |
| iPSC C4 - WT cell line | Boussaad et al. (2020) | N/A |
| iPSC C4 - SNCA KO | Barbuti et al. (2020a) | N/A |

(*Continued on next page*)

*Continued*

| REAGENT or RESOURCE | SOURCE | IDENTIFIER |
|---|---|---|
| Oligonucleotides | | |
| qRT-PCR Primers | See Table S1 | TibMolBio |
| siRNA Control A | Santa Cruz | Cat#sc-37007 |
| siRNA αsyn | Santa Cruz | Cat#sc-29619 |
| siRNA ACSL4 | Santa Cruz | Cat#sc-60619 |
| Recombinant DNA | | |
| Plasmid pSpCas9(BB)-2A-GFP (px458) | Addgene | Cat#48138 |
| Plasmid pX330-U6-Chimeric_BB-CBh-hSpCas9 | Addgene | Cat#42230 |
| Software and algorithms | | |
| Prism v9 | GraphPad Software | https://www.graphpad.com/scientific-software/prism/ |
| Kaluza | Beckman Coulter | https://www.beckman.fr/flow-cytometry/software/kaluza |
| FlowJo v10 | FlowJo, Treestar Inc. | https://www.flowjo.com |
| ImageJ | Java Source | https://imagej.nih.gov/ij/download.html |

## RESOURCE AVAILABILITY

### Lead contact

Further information and requests for resources and reagents should be directed to and will be fulfilled by the lead contact, David Devos (David.DEVOS@CHRU-LILLE.FR).

### Materials availability

All newly generated plasmids and LUHMES cell lines generated in this study are available from the lead contact without restriction. smNPC generated CRISPR cell lines are restricted due to an MTA.

### Data and code availability

- Phospholipid measurement datasets generated during this study have been deposited at Mendeley Data and are publicly available as of the date of publication. The DOI is listed in the key resources table.
- This paper does not report original code.
- Any additional information required to reanalyse the data reported in this paper is available from the lead contact upon request.

## EXPERIMENTAL MODEL AND SUBJECT DETAILS

### Cell lines

LUHMES cells were used in this study and kindly provided by Pr. Marcel Leist from the University of Konstanz. Stable LUHMES subclones lacking the main 140 α-syn isoform were generated by transfection of proliferative LUHMES cells with pSpCas9(BB)-2A-GFP (PX458) plasmid from Addgene (#48138). Small molecule derived neuronal precursor cells (smNPC) were differentiated from iPSC. Control smNPC line C4 - WT was previously described and characterised in (Boussaad et al., 2020), and C4 - *SNCA* KO iPSC were generated by transfection with the Cas9 plasmid pX330 (Addgene, 42,230). The *SNCA* triplication line was obtained from EBISC (cell line Edi001-A) and the isogenic gene corrected line (Iso WT) was generated and kindly provided by Dr Tilo Kunath from the University of Edinburgh (Mohamed et al., 2021).

## METHOD DETAILS

### Cell culture

For LUHMES cell culture, NunclonTM cell culture flasks and well-plates were coated with 50μg/ml of PLO and 1μg/ml fibronectin. Cells were grown at 37°C in a humidified 95% air, 5% CO2 atmosphere. Proliferating cells are maintained in advanced DMEM/F12 media supplemented with 1x N2, 2mM L-glut and 40ng/ml bFGF. For dopaminergic neuron differentiation, the proliferative media was replaced by differentiation media (advanced DMEM/F12, 1x N2, 2mM L-glut, 1mM dibutyryl cAMP, 1μg/mL tetracycline and 2ng/mL recombinant human GDNF). After 2 days of pre-differentiation, cells were harvested with trypsin, centrifuged for 5 min at

300g, counted and seeded in plates. LUHMES cells were left to fully differentiate for another 3 days in order to start every experimental protocol at day 5 of differentiation. All media were supplemented with 1% penicillin and streptomycin.

smNPC expansion medium consisted of N2B27 supplemented with CHIR, PMA and ascorbic acid (AA), with a medium change every other day. For splitting, cells were digested into single cells with a 15 min incubation at 37°C with prewarmed accutase (PAA). Cells were diluted and collected with DMEM and centrifuged at 200g for 5 min. The cell pellets was resuspended in fresh smNPC expansion medium and plated on Matrigel-coated culture plates. For generation of midbrain dopaminergic neurons, smNPC expansion medium was changed to N2B27 with 100ng/ml FGF8, 1μM PMA and 200μM AA. After 8 days, media was changed to maturation medium: N2B27 with 10ng/ml BDNF, 10ng/ml GDNF, 1ng/ml TGF-b3, 200μM AA and 500μM cAMP. Neuronal maturation and differentiation of smNPC was performed for at least 28 days to generate midbrain-specific dopaminergic neurons.

### *siRNA-mediated knock-down of α-syn and ACSL4*

siRNA transfection was performed by preparing solution A - RNAiMAX lipofectamine (ThermoFisher Scientific, 10,601,435) and OptiMEM (ThermoFisher Scientific, 10,149,832), and solution B consisting of siRNA (10μM) and OptiMEM. The siRNA control-A (sc-37007), a-syn (sc-29619) and ACSL4 (sc-60619) were purchased from SantaCruz Biotechnology. After 5 min of incubation, both solutions were combined and transferred to plates before seeding day 2 pre-differentiated LUHMES cells. Cells were left to fully differentiate for an additional 3 days before treatments. siRNA-mediated KD efficiency was measured by PCR and Western blot 72h post transfection.

For smNPC derived midbrain, the media was removed from seeded cells in 24-well plates and replaced by 400μL maturation media per well. The siRNA mix was prepared as follow: for 1 well, 1.5μL RNAiMAX lipofectamine was carefully mixed with 50μL OptiMEM and separately, 1.5μL of the control or a-syn siRNA were mixed with 50μL OptiMEM. The two solutions were left to incubate at room temperature for 5 min before carefully mixing vol:vol. The transfection solution was left to incubate at room temperature for an additional 15 min before adding 100μL per well. 6h later, 500μL of maturation was added to each well and cells were left for 72h before conducting any experimentation or extracting the RNA.

### *CRISPR/Cas9-mediated KO of 140 α-syn in LUHMES cells*

The experimental procedure for generating CRISPR/Cas9 clones on LUHMES cells was adapted from *Shah* et al. *(2016)*, with some minor alterations. CRISPR gRNA were designed by http://crispor.tefor.net/. The gRNA targeting exon 3 were inserted into pSpCas9(BB)-2A-GFP (PX458) plasmid from Addgene (#48138). Following gRNA ligation, OneShot *E.Coli* bacteria were transformed and spread on separate labeled LB agar plates in the presence of 50μg/ml ampicillin. Colonies were left to grow overnight at 37°C. The following day, 25 individual colonies were picked and PCR analysis was conducted to validate the plasmid sequence. The *SNCA* Ex3 gRNA oligonucleotide sequences are as follows:Sense (5′ to 3′): CACCgTggTgCATggTgTggCAAC.

Antisense (5′ to 3′): AAACgTTgCCACACCATgCACCACTo generate 140 a-syn KO clones, LUHMES cells were electroporated with PX458- *SNCA* Ex3 gRNA plasmids using the Amaxa P3 primary cell kit (V4XP-3024) on a nucleic acid transfection apparatus (4D Nucleofector device) with EM-110 program. Transfected cells were FACS sorted by fluorescence (FACSAria II, BD) into several 96-well plates. Single cell colonies were left to grow in proliferation media and amplified until frozen. The DNA was extracted for PCR amplification before sequence verification using the following primers:

Forward: 5' - gCTTgAgACTTATgTCTTgAATTTg

Reverse: 5′- TCTTgAATACTgggCCACAC Successfully edited clones were verified using Western blot.

### *CRISPR/Cas9-mediated SNCA KO in smNPC*

Control smNPC line C4 - WT was previously described and characterised in (Boussaad et al., 2020). C4 - *SNCA* KO iPSC were generated as described in (Barbuti et al., 2020a). Briefly, the Cas9 plasmid pX330 (Addgene, 42,230) containing a sgRNA targeting the human *SNCA* sequence gctgctgagaaaaccaaaca was transfected into C4 -WT cells. iPSCs were dissociated to single cells using PAA and plated in iPS media as described in (Barbuti et al., 2020b; Boussaad et al., 2020), plus Rho- Kinase Inhibitor Y-27632 (10μM, Abcam ab120129). 1 x 106 cells were then electroporated using the 2D-Amaxa nucleofector unit (Lonza, Basel, Switzerland) with program B16. After electroporation, 1mL of E8 was added to the cuvette before being placed at 37°C for 10 min. Cells were then plated into 6-well plates and cell selection was achieved using antibiotic resistance to puromycin when small to medium-sized colonies began to appear.

### *Cell viability via resazurin assay*

A stock solution was prepared at a concentration of 10mg/ml by dissolving resazurin dye (7-hydroxy-3H-phenoxazin-3-one 10-oxide) in $dH_2O$. Approximately $4x10^4$ LUHMES or mDANs were plated on coated 96-well plates in appropriate medium. Cytotoxicity was assayed 24 or 48h post treatment by adding resazurin solution (10% of cell culture volume per well – final concentration 100μg/ml) and cells were left to incubate for 2h at 37°C. Samples were analyzed fluorometrically on a microplate reader (Mithras LB950 or BioTek citation 5 imaging reader, Ex = 540nM, Em = 600nM). Background signals obtained from cell-free wells were subtracted from each sample. Cell viability under treatment conditions were reported as a percentage relative to untreated control cells.

### *Lipid peroxidation analysis via flow cytometry*

LUHMES cells were seeded at day 2 of differentiation in 24 well-plates at a density of 300,000 cells per well and left to complete the differentiation until day 5. Following ferroptosis induction, cells were collected following the addition of trypsin, centrifuged for 5 min at 300g and resuspended in 200μL PBS containing the LIVE/DEAD (Thermo Fisher - L23105) probe in order to differentially identify live and dead cells. Following a 15 min incubation at 37°C, an additional 200μL of PBS containing C11-BODIPY 581/591(Thermo Fisher - D3861) probe was added to the cells at a final concentration of 1μM. Cells were incubated for another 15 min at 37°C

and analyzed using the FORTESSA X20 flow cytometer (BD Biosciences). Data were collected from at least 10,000 cells and C11-BODIPY staining was measured in the living cell population. Data was analyzed using the Kaluza software. To report the percentage increase in lipid peroxidation, the increase fluorescence in the FITC channel was compared relative to control cells where basal lipid peroxidation levels were set to ~1% (Figure S7).

For smNPC derived midbrain neurons, lipid peroxidation measurements were conducted as described above with some minor alterations: Following treatment, cells were collected with prewarmed accutase and centrifuged at 500g for 5 min. Cells were resuspended in 300μL of PBS containing 2μM C11-BODIPY and incubated for 20 min at 37°C. For staining of viable cells, 17μg/ml DAPI was added to the cells immediately before measurement.

### Lipid extraction

Lipids were extracted from cells according to the method of *Folch* et al. *(1957)* (Folch et al., 1957). Briefly, 3 million cells were homogenized with 2mL of NaCl solution in water (0.73%). Lipids were extracted with 10 mL of $CHCl_3$/$CH_3OH$ (2:1, v/v), and vortexed for 1 min. Mixture was centrifuged at 3000 rpm for 3 min. The upper phase was discarded and the lower phase collected through a protein interface using a Pasteur pipette. After evaporation, the lipid extract (lower phase) was re-dissolved in 200μL of $CHCl_3$/$CH_3OH$ (2:1, v/v) and stored, under nitrogen, at −20°C until further analyses.

### Analysis of phospholipid molecular species

In the 200μL lipid extract, 10μL of internal standards mixture containing 320μg/ml PC(14:0/14:0) and 160μg/ml PE(14:0/14:0) were added. The process of identification and quantification of phospholipids species was performed on a Thermo UltiMateTM 3000 coupled to an Orbitrap Fusion Tribrid Mass Spectrometer equipped with an EASY-MAX NG Ion Source (H-ESI) (Thermo Scientific). Separation of phospholipid classes was achieved under HILIC conditions using Kinetex Hilic 100 × 2.1 mm, 1.7μm column (Phenomenex), with a flow of 0.500 mL.min$^{-1}$. The mobile phase consisted of (A) $CH_3CN$/$H_2O$ (96/4, v/v) containing 10 mM ammonium acetate and (B) $CH_3CN$/$H_2O$ (50/50, v/v) containing 10 mM ammonium acetate. The injection volume was 10 μL and the column was maintained at 50°C. PL species were detected by high resolution mass spectrometry (HRMS) analysis, and H-ESI source parameters were optimized and set as follows: ion transfer tube temperature of 285°C, vaporizer temperature of 370°C, sheath gas flow rate of 35 au, sweep gas of 1 au and auxiliary gas flow rate of 25 au. Positive and negative ions were monitored alternatively by switching polarity approach with a static spray voltage at 3500V and 2800V in positive and negative respectively. Mass spectra in full scan mode were obtained using the Orbitrap mass analyzer with the normal mass range and a target resolution of 240,000 (FWHM at m/z 200), on a mass range to charge ratio m/z form 200–1600 using a Quadrupole isolation on a normal mass range. All MS data were recorded using a max injection time of 100 ms, automated gain AGC target (%) at 112.5, RF lens (%) at 50 and one microscan. An Intensity Threshold filter of $1 \times 10^3$ counts was applied. For MS/MS analyses, data-dependent mode was used for the characterization of PL species. Precursor isolation was performed in the Quadrupole analyzer with an isolation width of m/z 1.6. Higher-energy Collisional Dissociation (HCD) was employed for the fragmentation of PL species with optimized stepped collision energy of 27%. The linear ion trap (LIT) was used to acquire spectra for fragment ions in data-dependent mode. The AGC target was set to $2 \times 10^4$ with a max injection time of 50 ms. All MS and MS/MS data were acquired in the profile mode. The Orbitrap Fusion was controlled by Xcalibur 4.1 software. Data of high accuracy and the information collected from fragmentation spectra, with the help of the LipidSearch software (Thermo) and the LIPID MAPS database (https://www.lipidmaps.org/) were used for PL species identification.

The index of peroxidability for PC and PE (PI = (% monoenoic FA × 0.025) + (% dienoic FA × 1) + (% trienoic FA × 2) + (% tetraenoic FA × 4) + (% pentaenoic FA×6) + (% hexaenoic FA × 8)) was calculated according to (Naudí et al., 2017).

### Western blot analysis

Cells were lysed in RIPA buffer containing 1% phosphatase and protease inhibitors for 15minutes at 4°C. Cells were fully lysed by sonicating for 15 s with 1 s impulses every 0.5s with an amplitude of 20%. Cell debris was removed by centrifugation at 1000g for 10 min, 4°C and protein concentration was determined using the Pierce BCA protein assay kit (ThermoFisher Scientific, 23,225). For Western blot analysis, samples were denaturated by heating at 90°C for 10 min in standard loading dye for SDS-Page and loaded on 4–20% SDS gels. Proteins were transferred onto nitrocellulose membranes. For optimal a-syn detection, blots were then fixed with 4%PFA for 30 min at room temperature before blocking with either 5% BSA TBS-Tween 20 (TBS-T) 0.1% or 5% NFDM TBS-T 0.05% (non-fat dry milk) for 1 h at room temperature. The blots were incubated with the indicated primary antibodies diluted in either 5% BSA TBS-T 0.1% or 5% NFDM TBS-T 0.05%, according to manufacturer's instructions, overnight at 4°C. The following day, primary antibodies were washed 3 × 5 min with TBS-T 0.1% and 3 × 5 min with TBS. Membranes were incubated with species-specific secondary antibodies conjugated to horseradish peroxidase which was detected by enhanced chemiluminescence with Amersham ECL detection reagents. Chemiluminescence signals were visualised with Fujifilm LAS (4000), and quantification of the signals was done using ImageJ with protein quantification normalized to β-actin signals.

### Quantitative reverse transcription PCR

Total RNA was extracted from differentiated cells in either 6 well-plates or 24 well-plates using the QIAGEN RNAeasy extraction kit according to manufacturer's instructions. Total RNA was dosed with BioSpec-nanodrop and a DNase step was performed on 2μg of total RNA before reverse transcription with Superscript II reverse Transcriptase (ThermoFisher Scientific, 18064022) using random primers (ThermoFisher Scientific, 48,190,011) in a 40μL reaction. PCR amplification of the cDNA was quantified using the LightCycler FastStart DNA Master SYBR Green I (Roche, 3,003,230). The housekeeping gene control was TBP. Primers were designed using NCBI primer design and purchased from TibMolBio. Threshold cycles were determined for each gene and expression levels were calculated relative to TBP. The sequences of the primers used for the qPCR are listed in Table S1.

### Quantification and statistical analysis

All quantitative data were shown as mean ± SEM and statistical analyses were performed using the Prism 9 GraphPad Software. The number of biological replicates for each experiment is indicates in the figure legends. Unless otherwise stated, differences between means were determined using the parametric two-tailed Student's *t*-tests and following data normality verification, and were considered significant at $p < 0.05$.